Mechanics Research Communications 113 (2021) 103671

Contents lists available at ScienceDirect

Mechanics Research Communications

journal homepage: www.elsevier.com/locate/mechrescom

Nonlinear subgrid-scale models employing the non-persistence-of-straining tensor

João R. Andrade[a,*], Ramon S. Martins[b], Roney L. Thompson[c], Aristeu S. Neto[a], Gilmar Mompean[d]

[a] Dep. of Mechanical Eng., Fed. Univ. of Uberlândia, Fluid Mech. Lab., Uberlândia, Minas Gerais, Brazil
[b] Dep. of Mechanical Eng., Universidade Vila Velha, Av. Comissário José Dantas de Melo, 21, Vila Velha, Brazil
[c] Dep. of Mechanical Eng., COPPE, Fed. Univ. of Rio de Janeiro, Ilha do Fundão, Rio de Janeiro, Brazil
[d] Univ. de Lille et Unité de Mécanique de Lille - UML EA 7512, Cité Scientifique, Villeneuve d'Ascq, France

ARTICLE INFO

Article history:
Received 16 October 2020
Revised 5 February 2021
Accepted 7 February 2021
Available online 9 February 2021

Keywords:
Tensor decomposition
Large Eddy Simulation
Nonlinear subgrid-scale closure model

ABSTRACT

Nonlinear subgrid-scale (SGS) models using the resolved rate-of-strain and non-persistence-of-straining tensors are assessed employing an *a priori* test for turbulent channel flows using Direct Numerical Simulation (DNS) results. The modeled and DNS subgrid stress tensors are compared. The results have shown that including the non-persistence-of-straining tensor in the tensorial basis of the SGS model leads to a better representation of the anisotropy of these scales. The near-wall region modeling can be significantly improved when compared to linear models that do not consider the non-persistence-of-straining tensor.

1. Introduction

Turbulence in fluid flows is a complex and nonlinear phenomenon involving three-dimensional vortex stretching. Due to the complex relation and interaction between the various characteristic quantities of this phenomenon, even the smallest turbulent structures (Kolmogorov structures) exert influence on the flow as a whole. Therefore, for the prediction of the velocity field, these small structures must be considered, demanding a high computational cost. To overcome this restriction and still maintain a reliable mathematical representation of this phenomenon, the Large Eddy Simulation (LES) method was formulated. This method was proposed based on the fact that in the small structures in high Re flows, Re, the turbulent structures present a more universal behavior.

In its first formulation, Smagorinsky [25] considered the hypothesis of proportionality between the modeled SGS stress tensor, $\boldsymbol{\tau}^M$, and the filtered rate-of-strain tensor, $\widetilde{\boldsymbol{S}}$. Despite reasonable results for several related cases, Smagorinsky's model fails when the turbulent flow is bounded by one or more solid surfaces, and the flow field becomes more complex. Due to this complexity added to the velocity field, the flow presents inhomogeneity and anisotropy that are responsible for the generation of an energy transfer in the physical space where the energy sources will behave differently depending on the distance from the wall [1]. The Smagorinsky's SGS model imposes an alignment of the eigenvectors and a proportionality of the eigenvalues of the modeled SGS stress and $\widetilde{\boldsymbol{S}}$. These restrictions lead to inconsistencies inherent to the structure of the corresponding model. Hence, special treatments are needed, especially in regions close to walls [6,17]. In other words, the eddy viscosity models based on the direct relationship between the modeled subgrid Reynolds stress tensor and rate-of-strain are poor and cannot predict correctly the exchange of turbulent kinetic energy between the resolved scales and the small structures. According to Meneveau and Katz [16], even by considering an exact turbulent viscosity field in the Smagorinsky closure model, $\boldsymbol{\tau}^M$ still could not be well predicted.

Due to the limitations found in the linear closure model, more complex subgrid models have been developed to improve the prediction of the SGS stress tensor, $\boldsymbol{\tau}$, and to capture the SGS anisotropy, see [4,15,22,30]. Silvis *et al* [24] proposed a systematic approach to develop SGS models where requirements were established to enhance the representation efficiency of the small unresolved scales.

Besides the traditional SGS methods depicted above, we can find other branches of LES. The Implicit LES (ILES) has the advantage of not needing explicit parameters, i.e. no SGS model is added to the filtered equations, and the numerical truncation is responsible for the energy balance in the highest wavenumbers. According to Margolin et al. [14], it is mainly applied to flows with high

* Corresponding author.
E-mail address: joao.andrade@ufu.br (J.R. Andrade).

https://doi.org/10.1016/j.mechrescom.2021.103671
0093-6413/

Table 1
Overview of DNS parameters.

Re_τ	$N_x \times N_y \times N_z$	δx^+	δy_w^+, $\delta y_{\max}^+$	δz^+
180	$512 \times 129 \times 128$	8.8	0.2, 7.1	6.6
590	$1536 \times 257 \times 512$	9.6	0.5, 10.4	5.4

Re. The Monotone Integrated LES (MILES) method, implicitly uses a suitable SGS model with a particular class of high-resolution methods [3]. Different kinds of analyses have shown a good correlation with experimental results [8]. In the case of Very LES (VLES), only the large, anisotropic scales are computed. Successes of VLES are reported by Orszag and Staroselsky [18]. The Temporal LES (TLES) approach uses filtered equations where a deconvolution method is applied to the time-domain [21]. Reasonable agreement with DNS was obtained by Thais et al. [26].

From the perspective of Reynolds Averaged Navier-Stokes Equations (RANS equations), several nonlinear closure models were proposed, e.g. [7,29]. Thompson *et al.* [29] proposed a new approach to evaluate the Reynolds stress dependence upon mean kinematic tensors and to measure the efficiency of a new closure model for RANS, where the non-persistence-of-straining tensor is employed to compose a nonlinear polynomial closure model. The combination of this tensor with the rate-of-strain tensor was shown to be able to predict anisotropies present in wall-bounded flows [29].

Since the first works using LES, experimental and DNS data sets have been extensively employed to test SGS models. This type of model test was introduced by Piomelli et al. [19] and was called as "*a priori* test". In the literature, many authors applied the *a priori* test in several situations, see [5,10,11,20,32].

In this context, the present work proposes and evaluates a novel nonlinear subgrid closure model based on the filtered field of the rate-of-strain and the non-persistence-of-straining tensor, a set of objective tensors. We employed DNS of turbulent plane channel flow at two different friction Reynolds numbers, namely, $Re_\tau = 180$ and 590. In order to predict the maximum correlation that the proposed model can achieve, a mathematical procedure is applied to determine the set of scalar coefficients based on the minimization of the discrepancy between the exact and the modeled SGS stress.

2. Direct numerical simulations

In order to establish SGS stress model evaluation, DNS simulations of fully developed turbulent plane channel flow were provided in the present work. Here we present the main characteristics of the applied code.

The Navier-Stokes equations is solved with periodic boundary conditions on a hybrid spatial scheme that includes Fourier spectral accuracy in two directions (x and z) and sixth-order compact finite differences for first and second-order wall-normal derivatives (y). Spatial averaging is taken in the two homogeneous channel direction (x, z). Convergence of the averaged data is evaluated according to Andrade et al. [2]. The full description of the employed algorithm can be found in Thais et al. [27].

Table 1 details the database parameters of the numerical simulations for the different *Re*. The presented parameters are *Re*, domain size, number of grid points, and mesh resolution.

3. Methodology

3.1. The novel nonlinear subgrid model

The present approach expresses the anisotropic part of $\boldsymbol{\tau}$ for LES as a function of the resolved rate-of-strain tensor $\widetilde{\boldsymbol{S}}$ and the resolved non-persistence-of-straining tensor $\widetilde{\boldsymbol{P}}$, where $\widetilde{\boldsymbol{P}}$ is given by.

$$\widetilde{\boldsymbol{P}} = \widetilde{\boldsymbol{S}} \cdot (\widetilde{\boldsymbol{W}} - \widetilde{\boldsymbol{\Omega}}^S) - (\widetilde{\boldsymbol{W}} - \widetilde{\boldsymbol{\Omega}}^S) \cdot \widetilde{\boldsymbol{S}}, \tag{1}$$

where $\widetilde{\boldsymbol{W}}$ is the skew-symmetric part of the mean velocity gradient (the mean vorticity tensor). $\widetilde{\boldsymbol{\Omega}}^S$ is the rate-of-rotation of the eigenvectors of $\widetilde{\boldsymbol{S}}$.

Then, the modeled deviatoric part of $\boldsymbol{\tau}$, $\boldsymbol{\tau}^M$, is expressed as function of $\widetilde{\boldsymbol{S}}$, $\widetilde{\boldsymbol{P}}$, and the grid dimension, Δ. A general form of the tensorial function can be obtained. It consists of a tensor polynomial expansion with six elements and its coefficients. By using the representation theorems, the most general model is given by:

$$\tau_{ij}^{M*} = \sum_{k=1}^{6} \beta_k T_{ij}^{(k)}, \tag{2}$$

where $\tau_{ij}^{M*} = \tau_{ij}^M - \frac{1}{3}\tau_{kk}^M \delta_{ij}$ and $T_{ij}^{(k)}$ are given by:

$$\begin{aligned} T_{ij}^{(1)} &= -\Delta^2 |\widetilde{\boldsymbol{S}}|^2 \delta_{ij} & T_{ij}^{(2)} &= \Delta^2 |\widetilde{\boldsymbol{S}}| \widetilde{S}_{ij} \\ T_{ij}^{(3)} &= \Delta^2 \widetilde{S}_{ik}\widetilde{S}_{kj} & T_{ij}^{(4)} &= \Delta^2 |\widetilde{\boldsymbol{P}}| \delta_{ij} \\ T_{ij}^{(5)} &= \Delta^2 \widetilde{P}_{ij} & T_{ij}^{(6)} &= \Delta^2 |\widetilde{\boldsymbol{P}}|^{-1} \widetilde{P}_{ik}\widetilde{P}_{kj}, \end{aligned} \tag{3}$$

and β_k are scalar coefficients, the tensor norms are given by $|\widetilde{\boldsymbol{S}}| = \sqrt{2\mathrm{tr}(\boldsymbol{S}^2)}$ and $|\widetilde{\boldsymbol{P}}| = \sqrt{2\mathrm{tr}(\boldsymbol{P}^2)}$.

This kinematic criterion $\widetilde{\boldsymbol{P}}$ is local, objective, and is not restricted to particular classes of flows. It has proven to well predict anisotropies that are present in turbulent flows [29]. Besides the characteristics listed above, it is worth mentioning that the non-persistence-of-straining tensor is orthogonal to $\widetilde{\boldsymbol{S}}$. In other words, it means that $\widetilde{\boldsymbol{P}}$ can attain regions in the tensorial space not reached by $\widetilde{\boldsymbol{S}}$.

The non-persistence-of-straining tensor captures the local characteristic of the flow to avoid being persistently stretched. In this sense, when this tensor vanishes the material filaments that are aligned with the eigenvectors of $\widetilde{\boldsymbol{S}}$ have the tendency to continue this alignment. However, a non-vanishing $\widetilde{\boldsymbol{P}}$indicates a stretch relieving in the sense that the material filaments aligned to the principal directions of $\widetilde{\boldsymbol{S}}$ tend to avoid this state. Therefore, as $\widetilde{\boldsymbol{S}}$ is increased, the local flow defies the directional tendency dictated by $\widetilde{\boldsymbol{S}}$.

Since the influence of each tensor in the tensorial basis from Eq. (2) is not yet known, five simpler models derived from the general form can be proposed. The simplified models comes from the fact that, regarding RANS approach, the set of tensor basis composed by $\boldsymbol{S}$, $\boldsymbol{SS}$, $\boldsymbol{P}$ and $\boldsymbol{PP}$ is able to totally reproduce the anisotropic Reynolds stress [29]. The proposed Models $I - V$ are given by the following expression:

$$\begin{aligned} \tau_{ij}^{I*} &= -\beta_2 T_{ij}^{(2)}, \\ \tau_{ij}^{II*} &= \beta_1 T_{ij}^{(1)} - \beta_2 T_{ij}^{(2)} + \beta_3 T_{ij}^{(3)}, \\ \tau_{ij}^{III*} &= \beta_1 T_{ij}^{(1)} - \beta_2 T_{ij}^{(2)} + \beta_3 T_{ij}^{(3)} + \beta_5 T_{ij}^{(5)}, \\ \tau_{ij}^{IV*} &= -\beta_2 T_{ij}^{(2)} + \beta_5 T_{ij}^{(5)}, \\ \tau_{ij}^{V*} &= -\beta_2 T_{ij}^{(2)} + \beta_4 T_{ij}^{(4)} + \beta_5 T_{ij}^{(5)} + \beta_6 T_{ij}^{(6)}. \end{aligned} \tag{4}$$

where the superscript $(\,)^*$ indicates the deviatoric part of a tensor.

It is worth mentioning that Model I become the Smagorinsky's model by considering $\beta_2 = 2C_S^2$.

3.2. A priori *test in turbulent plane channel flow*

By means of the *a priori* test, the modeled SGS stress $\boldsymbol{\tau}^M$ must be evaluated based solely on the velocity field $\widetilde{u}_i$ sampled on the coarse grid (of mesh size $\widetilde{\Delta}$) used in the filtering process. Due to this fact, firstly it is needed to split the velocity field into resolved and SGS components by calculating $\widetilde{u}_i$ and $\widetilde{u_i u_j}$ where the tilde $\widetilde{()}$

is a filter at scale $\widetilde{\Delta}$. Several sensible choices for the functional form of the spatial low-pass filter, G, can be found in the literature; e.g. [16,31]. In the present work, the filtering operation is made by using the box filter in the homogeneous (periodic) directions. The box filter is applied to a grid with sides of length $\widetilde{\Delta} = (a/b)\Delta$ where $\widetilde{\Delta}$ is the mesh spacing in the current node of the coarse grid and $a > b$.

Three different resolutions of coarse grids were applied. Their grid spacing is about two, four, and eight times the grid spacing of the corresponding DNS grid, i.e. $\widetilde{\Delta} = \{2\Delta, 4\Delta, 8\Delta\}$.

Since we are dealing with a turbulent plane channel flow, the model coefficients β_k (Eq. (2)) found in the *a priori* test are assumed to be constants in time and in wall-parallel planes (xz) and vary only in the wall-normal direction as a function of the wall distance (y). Then, by setting the β_k to be constant on plane xz, the model coefficients are updated and are given by $C_k(y) = \langle \beta_k(x, y, z) \rangle$, where $\langle\,\rangle$ is the average computed in the xz-plane. Thus, Eq. (2) Is given by:

$$\begin{aligned}\tau_{ij}^{M*} = &-C_1\Delta^2|\widetilde{\boldsymbol{S}}|^2\delta_{ij} + C_2\Delta^2|\widetilde{\boldsymbol{S}}|\widetilde{S}_{ij} \\ &+ C_3\Delta^2\widetilde{S}_{ik}\widetilde{S}_{kj} + C_4\Delta^2|\widetilde{\boldsymbol{P}}|\delta_{ij} \\ &+ C_5\Delta^2\widetilde{P}_{ij} + C_6\Delta^2|\widetilde{\boldsymbol{P}}|^{-1}\widetilde{P}_{ik}\widetilde{P}_{kj}. \end{aligned} \tag{5}$$

The developed procedure to determine C_k coefficients is described next.

3.3. Model coefficients estimation based on SGS local error

The general and complete SGS model depends on unknown coefficients that are required to estimate the energetic influence of the SGS on the mean flow. In order to compute these coefficients, a SGS local error tensor $\boldsymbol{E}^\tau$ can be defined by computing the difference between the modeled and the exact SGS stress, i.e. $\boldsymbol{E}^\tau = \boldsymbol{\tau}^M - \boldsymbol{\tau}$.

We now introduce the SGS local quadratic error function, $\mathcal{Q}^\tau = \mathrm{tr}(\boldsymbol{E}^\tau \cdot \boldsymbol{E}^\tau)$. In order to apply the least square method [12] to minimize $\boldsymbol{E}^\tau$, we set $\partial\mathcal{Q}^\tau/\partial C_k = 0$ for each coefficient from Eq. (5). It leads to a set of six mathematical expressions which gives rise to a system of linear equations that can be solved to estimate the model coefficients:

$$\begin{bmatrix} \langle T_{ij}^{(1)}T_{ij}^{(1)}\rangle & \cdots & \langle T_{ij}^{(1)}T_{ij}^{(6)}\rangle \\ \langle T_{ij}^{(2)}T_{ij}^{(1)}\rangle & \cdots & \langle T_{ij}^{(2)}T_{ij}^{(6)}\rangle \\ \vdots & \ddots & \vdots \\ \langle T_{ij}^{(6)}T_{ij}^{(1)}\rangle & \cdots & \langle T_{ij}^{(6)}T_{ij}^{(6)}\rangle \end{bmatrix} \begin{Bmatrix} C_1 \\ C_2 \\ \cdots \\ C_6 \end{Bmatrix} = \begin{Bmatrix} \langle \tau_{ij}T_{ij}^{(1)}\rangle \\ \langle \tau_{ij}T_{ij}^{(2)}\rangle \\ \vdots \\ \langle \tau_{ij}T_{ij}^{(6)}\rangle \end{Bmatrix}. \tag{6}$$

Since the model coefficients are set to depend on the wall-distance y, the averaging operation in the wall parallel plans are applied to Eq. (6).

Eq. (6) is designated for the general model with the whole set of proposed tensor basis, i.e. $\widetilde{\boldsymbol{S}}$, $\widetilde{\boldsymbol{S}}\widetilde{\boldsymbol{S}}$, $\widetilde{\boldsymbol{P}}$, $\widetilde{\boldsymbol{P}}\widetilde{\boldsymbol{P}}$ and $\boldsymbol{I}$. However, from the proposed nonlinear SGS model it is possible to derive simpler models with a smaller set of tensor basis. For instance, we can propose the Model *I* by keeping only the $\widetilde{\boldsymbol{S}}$ to represent the modeled SGS. Then we have $\tau_{ij}^{M*} = C_2 T_{ij}^{(2)}$, where $C_2 = \langle \tau_{ij}T_{ij}^{(2)}\rangle / \langle T_{ij}^{(2)}T_{ij}^{(2)}\rangle$.

Following the same procedure from Model *I*, it is possible to estimate the coefficients for the Models *II*, *III*, *IV*, and *V*. Results presenting the evaluation of Models *I* to *V* are given in the following section.

4. Results

Herein, we present and compare the exact and the $\boldsymbol{\tau}^M$ components depending on the filtering grid and the *Re*. In order to analyze the correlation between both tensors, a normalized parameter, R_M, is employed. This parameter measures how important is the tensor $\boldsymbol{\tau}^M$ when compared with tensor $\boldsymbol{\tau}$ and can be found in Thompson [28]. Its quantity varies from 0 (orthogonality) to 1 (congruence), depending on the correlation between both tensors. All variables presented in the results section are averaged in several parallel-to-wall plans, varying on the wall-distance. The averaged variables are presented as $\langle\phi\rangle$, where ϕ is a generic variable.

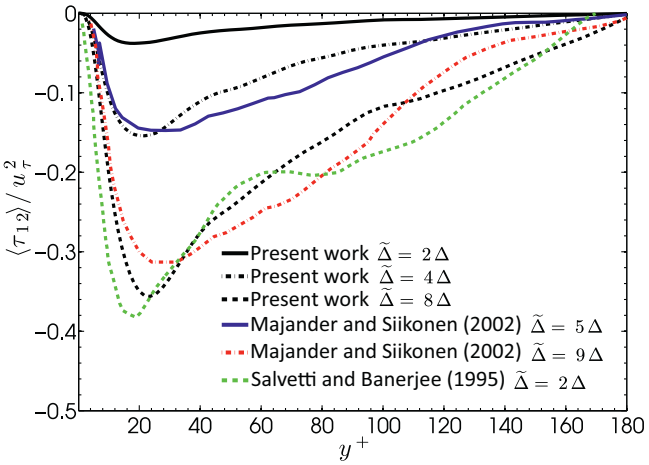

Fig. 1. Profile of τ_{12} scaled by u_τ^2 across channel half-width at $Re_\tau = 180$ compared to Majander and Siikonen [13] and Salvetti and Banerjee [23].

4.1. Filtered data

Regarding the influence of the filtering process in the modeled SGS stress tensor, Fig. 1 reports the comparison of the exact stress components τ_{12} at $Re_\tau = 180$ with results of Majander and Siikonen [13] and Salvetti and Banerjee [23], where $\tau_{ij} = \widetilde{u_i u_j} - \widetilde{u}_i\widetilde{u}_j$.

It can be noted that the peak of the τ_{12}, localized at $y^+ \approx 22$, is close to the reference results. In all cases, τ_{12} reaches a peak at the buffer layer and decreases at the same rate, vanishing at the center of the channel. As expected, the buffer layer has shown to be the most important region, where are found the peak of turbulent kinetic energy and the maximum ratio of production to dissipation of the turbulent kinetic energy [1].

In order to analyse the results, we define four different regions depending on y^+, i.e., I - viscous sublayer ($0 < y^+ < 5$), II - buffer layer ($5 < y^+ < 30$), III - log-law region ($y^+ > 30$) and IV – outer layer ($y^+ > 50$).

According to Cimarelli and De Angelis [4], the most important feature of the SGS models should be their ability to accurately reproduce the energy transfer between resolved and SGS scales ($\mathcal{P}_r = \tau_{ij}\widetilde{S}_{ij}$). In a wall-bounded turbulent flow, the physical process of $\mathcal{P}_r$ can behave very differently depending on the range of scales removed by the filter and on the wall-distances considered [9]. To evaluate the different behavior of $\mathcal{P}_r$, Fig. 2 presents the comparison of turbulent kinetic energy transfer from the large to the small structures $\mathcal{P}_r$ for different filter widths at $Re_\tau = 590$.

Results for $Re_\tau = 180$ were omitted since, apart from the peak intensity, no significant difference was observed between $Re_\tau = 180$ and $Re_\tau = 590$, with each peak located in the same region ($y^+ \approx 10$) in the buffer layer. This analysis is in accordance with the results of Andrade et al. [1]. With respect to the filtering influence, it is apparent that in a coarser grid, the energy injected in the SGS scales is larger. This result can be explained by the fact that for a coarser grid, the modeled spectral range is larger and, consequently, the energy change is higher.

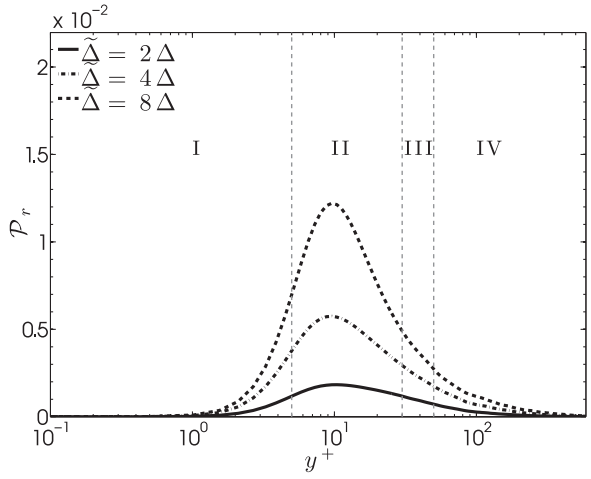

Fig. 2. Profile of $\mathcal{P}_r$ across the channel half-width at $Re_\tau = 590$.

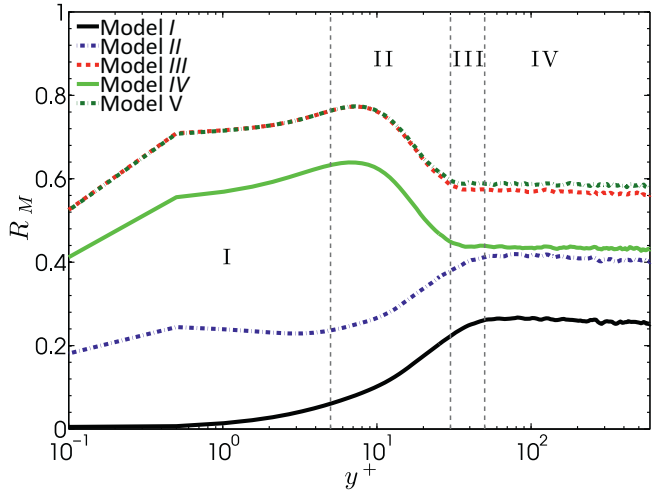

Fig. 3. Correlation coefficient, R_M, applied to Models *I* to *V* at $Re_\tau = 590$.

4.2. Nonlinear subgrid (SGS) model

In what follows, we conduct an analysis of the proposed nonlinear SGS models. As was described in Section 3.1, five models were proposed based on the complete tensorial basis. Except for the peak intensity, no great differences were found between the different filtering width and *Re*. Hence, in this section we show results for filter $\widetilde{\Delta} = 4\Delta$ and $Re_\tau = 590$.

The correlations between the exact and $\boldsymbol{\tau}^M$, R_M, are illustrated in Fig. 3. This set of analyses investigates how close the modeled tensor can get to $\boldsymbol{\tau}$.

These tests revealed that there is an important gain in the correlation between $\boldsymbol{\tau}$ and $\boldsymbol{\tau}^M$ when a more complex nonlinear SGS model is applied. From this figure, we can notice that the Models *III* and *V* present the most significant positive correlation. They reach a maximum value of $R_M \approx 0.76$ and a minimum of $R_M \approx 0.53$. Model *I*, the linear SGS model, was found to be the worst one. The black curve in Fig. 3 shows that the correlation tends to zero around the viscous sublayer regions with a maximum value of $R_M \approx 0.24$ at the outer layer.

This result indicates the poor correlation between $\boldsymbol{\tau}$ and $\widetilde{\boldsymbol{S}}$ in the whole channel, reaching the lowest values in the near-wall region. This behavior can be attributed to the highly anisotropic behavior of the smallest scales in the region [1]. These results were expected since Model *I* imposes an eigenvector alignment

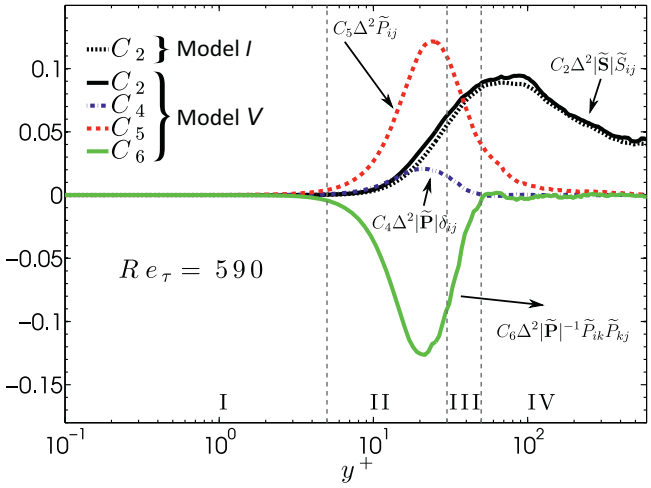

Fig. 4. Coefficients for SGS model for Models *I* and *V*.

and eigenvalues proportion between the SGS stress and the resolved rate-of-strain tensor. The correlation coefficient of Model *II* is better than the Model *I* uniformly throughout the channel. In this model, the eigenvector alignment between $\boldsymbol{\tau}$ and $\widetilde{\boldsymbol{S}}$ is imposed, but there is no proportion between its eigenvalues.

For Models *III*, *IV*, and *V*, we observe a great improvement of the correlation coefficient, mainly in the region close to the wall, where R_M reaches a peak in the buffer layer. These models (III, IV, and V) are the ones that include the tensor $\widetilde{\boldsymbol{P}}$ in their composition. On the basis of this evidence, it seems fair to suggest that this was the most remarkable result to emerge from the DNS data since by incorporating the non-persistence-of-straining tensor to the tensorial basis of the SGS model, the near-wall region was satisfactorily captured and considerably improved with respect to the linear model.

To assess the correlation coefficient R_M, it was necessary to compute the model coefficients C_k. Fig. 4 presents C_k for Models *I* and *V*, the worst and the best models, respectively.

Model *V* is composed by more components in its tensorial basis than Model *I*. One can notice that the coefficient C_2 for both models (I and V) have similar behavior. This fact indicates that the tensors $|\widetilde{\boldsymbol{P}}|\delta_{ij}$, $\widetilde{P}_{ij}$ and $|\widetilde{\boldsymbol{P}}|^{-1}\widetilde{P}_{ik}\widetilde{P}_{kj}$ do not affect the role of the tensor $|\widetilde{\boldsymbol{S}}|\widetilde{S}_{ij}$ in the SGS model. It is possibly explained by the property of orthogonality between $\widetilde{\boldsymbol{S}}$ and $\widetilde{\boldsymbol{P}}$, as was mentioned in the Section 3.1.

It can also be seen that coefficient C_2 tends to be more important in the outer layer whereas the other coefficients have their peaks in the buffer layer. This result is consistent with previous ones from literature, for which it was found that the tensor $\boldsymbol{P}$ promotes a better improvement in the buffer layer [29].

Fig. 5 compares the $\langle\tau_{11}\rangle$ and $\langle\tau_{12}\rangle$ components of the SGS tensor as predicted by Model *I* and Model *V* for the case at $Re_\tau = 590$ with the "exact" SGS tensor obtained from the DNS.

From this figure, we can observer that the exact $\langle\tau_{11}\rangle$ component is positive and reaches its peak at $y^+ \approx 11$, while $\langle\tau_{12}\rangle$ is always negative and has its maximum intensity at $y^+ \approx 25$. Concerning $\langle\tau_{11}\rangle$, it was found dramatic differences between Model *I* and the exact data, since this model predicts a negligible normal 11-component. On the other hand, Model *V* shows a peak of similar magnitude at a point near the one of the exact tensor. We observe from Fig. 5-(b) that both models are quite similar to the exact $\langle\tau_{12}\rangle$-component. This finding confirms the importance of the non-persistence-of-straining tensor in the composition of the modeled SGS stress tensor basis.

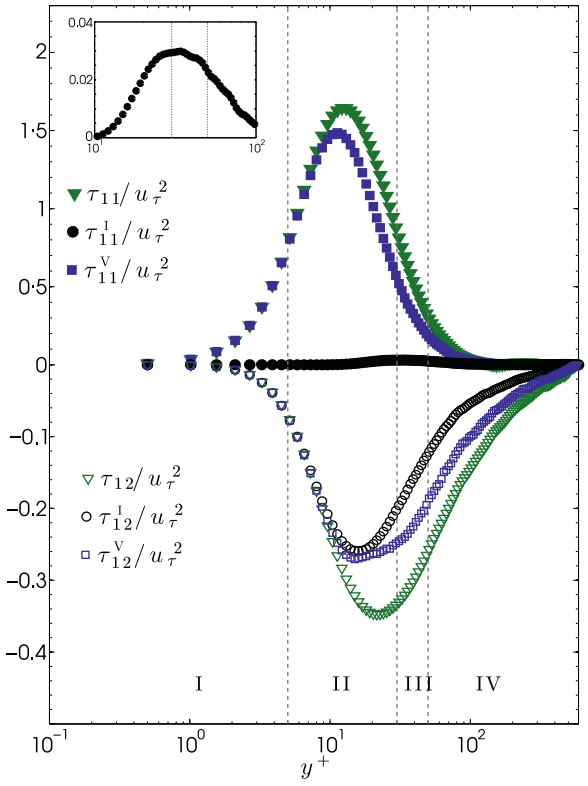

Fig. 5. Modeled and exact components of SGS stress tensor by applying Model *I* and Model *V*.

5. Conclusions

In the present work, we investigated the influence of nonlinear modeling of $\boldsymbol{\tau}$ by means of an *a priori* test using DNS data of turbulent plane channel flows. The novel nonlinear subgrid model for large eddy simulation includes combinations of the filtered rate-of-strain and the filtered non-persistence-of-straining tensors, both objective tensors.

By analyzing the linear closure model employing the rate-of-strain, it was showed that the SGS model composed by only $\widetilde{\boldsymbol{S}}$ (Smagorinsky model) is not an adequate assumption, mainly in the near-wall region, even when an ideal and exact distribution field of the turbulent viscosity is applied. This behavior can be explained by the poor prediction of the SGS anisotropy when the rate-of-strain is employed.

The addition of nonlinear terms in the description of the SGS stress model was able to represent more faithfully the exact SGS tensor as obtained by DNS. We can highlight that the inclusion of the non-persistence-of-straining tensor was crucial for capturing the normal components of the SGS tensor.

This result can be considered a significant improvement since a higher correlation is obtained in the near-wall region, where most closure models fail. Therefore, the proposed model possesses a great potential to predict a more accurate dissipation of energy in regions of high complexity. The findings of the present study suggest that by using a more complete SGS model, the dissipation of the turbulent kinetic energy is better estimated, since we impose neither alignment between the eigenvectors nor proportionally between the eigenvalues of $\boldsymbol{\tau}^M$ and $\widetilde{\boldsymbol{S}}$. It is worth mentioning that the closure models applied in the present work are solely based on an objective tensorial basis, i.e. invariant under changes of the reference frame.

Declaration of Competing Interest

The authors declare that they have no known competing financial interests or personal relationships that could have appeared to influence the work reported in this paper.

Acknowledgments

This research has granted access to the HPC resources of IDRIS under the allocation i20162b2277 made by GENCI. We would like to thank the support given by the Brazilian funding agency CNPq.

References

[1] J.R. Andrade, R.S. Martins, L. Mompean G. Laurent Thais, T.B. B. Gatski, Analyzing the spectral energy cascade in turbulent channel flow, Phys. Fluids 30 (6) (2018) 065110.
[2] J.R. Andrade, R.S. Martins, R.L. Thompson, G. Mompean, A. Silveira-Neto, Analysis of uncertainties and convergence of the statistical quantities in turbulent wall-bounded flows by means of a physically based criterion, Phys. Fluids 30 (4) (2018) 045106.
[3] J.P. Boris, F.F. Grinstein, E.S. Oran, R.L. Kolbe, New insights into large eddy simulation, Fluid Dyn. Res. 10 (199–228) (1992) 2–6, doi:10.1016/0169-5983(92)90023-P.
[4] A. Cimarelli, E. De Angelis, The physics of energy transfer toward improved subgrid-scale models., Phys. Fluids 26 (5) (1994) 055103.
[5] G. De Stefano, O.V. Vasilyev, D.E. Goldstein, A-priori dynamic test for deterministic/stochastic modeling in large-eddy simulation of turbulent flow, Comput. Phys. Commun. 169 (1–3) (2005) 210–213, doi:10.1016/j.cpc.2005.03.047.
[6] J.W. Deardorff, A numerical study of three-dimensional turbulent channel flow at large Reynolds numbers, J. Fluid Mech. 41 (1970) (1970) 453–480, doi:10.1017/S0022112070000691.
[7] T.B. Gatski, C.G. Speziale, On explicit algebraic stress models for complex turbulent flows, J. Fluid Mech. 254 (1993) 59–78.
[8] F. Grinstein, J. Boris, O. Griffin, Passive pressure-drag control in a plane wake, AIAA J. 29 (1991) 1436–1442.
[9] C. Härtel, L. Kleiser, F. Unger, R. Friedrich, Subgrid-scale energy transfer in the near–wall region of turbulent flows., Phys. Fluids 6 (9) (1994) 3130.
[10] A. Keating, U. Piomelli, E. Balaras, H.J. Kaltenbach, A priori and a posteriori tests of inflow conditions for large-eddy simulation, Phys. Fluids 16 (12) (2004) 4696–4712, doi:10.1063/1.1811672.
[11] E. Labourasse, D. Lacanette, A. Toutant, P. Lubin, S. Vincent, O. Lebaigue, J.P. Caltagirone, P. Sagaut, Towards large eddy simulation of isothermal two-phase flows: governing equations and a priori tests, Int. J. Multiph. Flow 33 (1) (2007) 1–39, doi:10.1016/j.ijmultiphaseflow.2006.05.010.
[12] D. Lilly, A proposed modification of the Germano subgrid-scale closure method., Phys. Fluids 4 (3) (1992) 633–635.
[13] P. Majander, T. Siikonen, Evaluation of Smagorinsky-based subgrid-scale models in a finite-volume computation, Int. J. Numer. Methods Fluids 40 (6) (2002) 735–774, doi:10.1002/fld.374.
[14] L.G. Margolin, W.J. Rider, F.F. Grinstein, Modeling turbulent flow with implicit LES, J. Turbul. 7 (2006) 1–27, doi:10.1080/14685240500331595.
[15] L. Marstorp, G. Brethouwer, O. Grundestam, A.V. Johansson, Explicit algebraic subgrid stress models with application to rotating channel, J. Fluid Mech. 639 (2009) 403–432.
[16] C. Meneveau, J. Katz, Scale-invariance and turbulence models for large-eddy simulation, Annu. Rev. Fluid Mech. 32 (2000) 1–32, doi:10.1146/annurev.fluid.32.1.1.
[17] P. Moin, J. Kim, Numerical investigation of turbulent channel flow, J. Fluid Mech. 118 (1982) 341–377, doi:10.1017/S0022112082001116.
[18] S.A. Orszag, I. Staroselsky, Cfd: progress and problems, Comput. Phys. Commun. 127 (2000) 165–171.
[19] U. Piomelli, P. Moin, J.H. Ferziger, Model consistency in large eddy simulation of turbulent channel flows., Phys. Fluids 31 (7) (1988) 1884.
[20] U. Piomelli, W.H. Cabot, P. Moin, S. Lee, Subgrid-scale backscatter in turbulent and transitional flows., Phys. Fluids A 3 (7) (1991) 176.
[21] C.D. Pruett, T.B. Gatski, C.E. Grosch, W.D. Thacker, The temporally filtered Navier-Stokes equations: properties of the residual stress, Phys. Fluids 15 (8) (2003) 2127–2140, doi:10.1063/1.1582858.
[22] W. Rozema, H.J. Bae, P. Moin, R. Verstappen, Minimum-dissipation models for large-eddy simulation, Phys. Fluids 27 (8) (2015) 085107, doi:10.1063/1.4928700.
[23] M.V. Salvetti, S. Banerjee, A priori tests of a new dynamic subgrid-scale model for finite-difference large-eddy simulations., Phys. Fluids 7 (11) (1995) 2831.
[24] M.H. Silvis, R.A. Remmerswaal, R. Verstappen, Physical consistency of subgrid-scale models for large-eddy simulation of incompressible turbulent flows, Phys. Fluids 29 (1) (2017) 015105, doi:10.1063/1.4974093.
[25] J. Smagorinsky, General circulation experiments with the primitive equations. I. The basic experiment., Mon. Weather Rev. 91 (1963) 99—164.
[26] L. Thais, A.E. Tejada-Martínez, T.B. Gatski, G. Mompean, Temporal large eddy simulations of turbulent viscoelastic drag reduction flows, Phys. Fluids 22 (1) (2010) 1–13, doi:10.1063/1.862466.

[27] L. Thais, A.E. Tejada-Martínez, T.B. Gatski, G. Mompean, A massively parallel hybrid scheme for direct numerical simulation of turbulent viscoelastic channel flow, Comput. Fluids 43 (1) (2011) 134–142, doi:10.1016/j.compfluid.2010.09.025.
[28] R.L. Thompson, Some perspectives on the dynamic history of a material element, Int. J. Eng. Sci. Technol. 46 (2008) 224–249.
[29] R.L. Thompson, G. Mompean, L. Thais, A methodology to quantify the nonlinearity of the Reynolds stress tensor, J. Turbul. 11 (33) (2010) 1–27.
[30] R. Verstappen, How much eddy dissipation is needed to counterbalance the nonlinear production of small, unresolved scales in a large-eddy simulation of turbulence? Comput. Fluids 176 (2018) 276–284.
[31] B. Vreman, B. Geurts, H. Kuerten, On the formulation of the dynamic mixed subgrid- scale model., Phys. Fluids 6 (12) (1994) 4057.
[32] B. Vreman, B. Geurts, H. Kuerten, A priori tests of large eddy simulation of the compressible plane mixing layer, J. Eng. Math. 29 (1995) 299–327, doi:10.1007/BF00042759.